Nuclear Instruments and Methods in Physics Research A 675 (2012) 78–83

Contents lists available at SciVerse ScienceDirect

Nuclear Instruments and Methods in Physics Research A

journal homepage: www.elsevier.com/locate/nima

Energy and resolution calibration of NaI(Tl) and $LaBr_3$(Ce) scintillators and validation of an EGS5 Monte Carlo user code for efficiency calculations

R. Casanovas [a,*], J.J. Morant [b], M. Salvadó [a]

[a] Unitat de Física Mèdica, Facultat de Medicina i Ciències de la Salut, Universitat Rovira i Virgili, ES-43201 Reus (Tarragona), Spain
[b] Servei de Protecció Radiològica, Facultat de Medicina i Ciències de la Salut, Universitat Rovira i Virgili, ES-43201 Reus (Tarragona), Spain

ARTICLE INFO

Article history:
Received 30 December 2011
Received in revised form
23 January 2012
Accepted 5 February 2012
Available online 10 February 2012

Keywords:
Scintillation gamma-ray spectrometry
NaI(Tl)
$LaBr_3$(Ce)
Energy calibration
Resolution calibration
Monte Carlo simulation
Efficiency calculation

ABSTRACT

The radiation detectors yield the optimal performance if they are accurately calibrated. This paper presents the energy, resolution and efficiency calibrations for two scintillation detectors, NaI(Tl) and $LaBr_3$(Ce). For the two former calibrations, several fitting functions were tested. To perform the efficiency calculations, a Monte Carlo user code for the EGS5 code system was developed with several important implementations. The correct performance of the simulations was validated by comparing the simulated spectra with the experimental spectra and reproducing a number of efficiency and activity calculations.

1. Introduction

Scintillation detectors, with a special emphasis on the NaI(Tl) detectors, have been broadly used in many fields over the last 50 years [1]. Recently, the new lanthanum-based scintillators have become commercially available [2]. Compared with the NaI(Tl) detectors, the lanthanum detectors have better scintillation properties, including energy resolution, temperature performance, decay time, light yield and material density [2]. All of these capabilities make lanthanum detectors good candidates to substitute the NaI(Tl) scintillators in most applications.

Nonetheless, the correct performance of all radiation detectors requires the correct calibration. When the scintillation detectors are used for gamma spectrometry, the calibration procedure can be divided into three sub-calibrations [3]: the energy calibration, the resolution calibration and the efficiency calibration. These calibrations make it possible to correctly identify and determine the activity of the involved isotopes.

However, while the energy and the resolution calibrations are easily performed experimentally, the efficiency calibration can be a demanding task, especially for complex and extended source geometries. Thus, a common approach to perform the efficiency calibration is to use the Monte Carlo (MC) simulation techniques, which must be experimentally validated at least for the simple source geometries. This validation enables one to extrapolate the simulations to obtain the efficiency curves for other sources that would be difficult or impossible to obtain in a laboratory.

In this study, we perform the energy and the resolution calibrations for the NaI(Tl) and $LaBr_3$(Ce) scintillators, and we test several fitting functions used in both calibrations. For the efficiency calculations, we present an MC user code, which is validated with certified calibration sources. The details of the more important implementations of the MC code are also discussed.

2. Materials and methods

2.1. Experimental setup

The detectors used in this study were a $2'' \times 2''$ NaI(Tl) and a $2'' \times 2''$ $LaBr_3$(Ce) scintillation detectors. The NaI(Tl) detector was an ORTEC® Model 905-3 and the $LaBr_3$(Ce) detector was a BrilLanCe™380 from Saint-Gobain Crystals. Both detectors were coupled to a preamplifier (ORTEC® Model 276) and an amplifier (ORTEC® Model 575A), which were connected to a multichannel pulse-height analyser ORTEC® TRUMP™-PCI-2k. The spectrum analysis software that we used was ScintiVision™ from ORTEC®.

The experimental data were obtained from five radioactive sources that allowed the coverage of all gamma energies up to 1408 keV. Table 1 shows the current activity (deduced from the

* Corresponding author. Tel.: +34977759382; fax: +34977759322.
E-mail address: ramon.casanovas@urv.cat (R. Casanovas).

0168-9002/$ - see front matter © 2012 Elsevier B.V. All rights reserved.
doi:10.1016/j.nima.2012.02.006

Table 1
Radioactive sources used in this study with their current activity and their active dimensions.

Radionuclide	Current activity[a] (kBq)	Source shape	Active dimensions (mm)
^{241}Am	3.2 ± 0.3	Squared	Side = 55
^{133}Ba	1.0 ± 0.1	Circular	Radius = 47
^{137}Cs	4.0 ± 0.4	Circular	Radius = 0.5
^{60}Co	1.40 ± 0.14	Circular	Radius = 1.0
^{152}Eu	Unknown	Unknown	Unknown

[a] At the time of measurement.

certifications) and the active dimensions of each source. In all measurements, the background spectra were subtracted. The data related to the decay, the energies and the emission probabilities were taken from [4].

2.1.1. Energy calibrations

The energy calibration consists of establishing a relationship between the channels C and the corresponding gamma-ray energies E in the spectrum. Because this relationship is not always linear [5], as expected, its nonlinearity may produce inaccuracies in the determination of the peak energies and the comparison of real spectra with the MC simulations. This nonlinearity is produced as a consequence of the different uncertainties introduced in the measured energies that come from the different processes involved in the detection of gamma-rays [1].

Thus, the relationship between the energy E and the peak position C should be extended to a polynomial with $n > 1$:

$$E = \sum_{k=0}^{n} a_k \cdot C^k \tag{1}$$

where n is the degree of the polynomial.

2.1.2. Resolution calibrations

The non-proportional light response in scintillation detectors is the main cause of the limited energy resolution [1,6–8]. This limitation makes it necessary to perform a peak width calibration, which establishes a correspondence between the peak width and its energy. Resolution calibrations are necessary as an input not only for the peak-analysis software but also for the MC simulations to obtain realistic spectra. Because the peak width is often given by the Full Width at Half Maximum (FWHM), this calibration establishes the dependence of the FWHM on the energy E, i.e., it sets the function FWHM(E). However, there is no consensus in the literature on the mathematical form of this function. Thus, we tested several functions to identify one that provides the best fit (see Table 3).

2.1.3. Experimental efficiency calibrations

The relationship between the number of counts under a peak and the activity of a radioactive source is set by the efficiency calibration. Whereas the two previous calibrations only depended on the gamma-ray energy, the efficiency calibration depends on many other factors, such as the source-to-detector distance, the source geometry and the materials surrounding the setup. Consequentially, the efficiency calibration is only valid for identical calibration and measuring conditions.

If the efficiency calibrations are performed with certified sources, the experimental efficiencies ε_{exp} are calculated using the following equation:

$$\varepsilon_{exp} = \frac{N}{A \cdot t \cdot p} \tag{2}$$

where N is the number of net counts under the full-energy peak, A is the known radionuclide activity, t is the counting time and p is the emission probability of the particular gamma-ray being measured.

The uncertainty propagation gives the following equation for the efficiency uncertainty $\delta\varepsilon_{exp}$:

$$\delta\varepsilon_{exp} = \varepsilon_{exp}\sqrt{\left(\frac{\delta N}{N}\right)^2 + \left(\frac{\delta A}{A}\right)^2 + \left(\frac{\delta p}{p}\right)^2} \tag{3}$$

2.2. Monte Carlo simulation

The MC simulations were performed with the EGS5 code system [9]. This general-purpose package enables the simulation of the coupled transport of electrons and photons in an arbitrary geometry. The EGS5 subroutines are controlled by a user code, which must be written in Fortran 77. The user code must contain all of the information about the radiation source (the type of particles, the energy and the probabilities of emission, the position and the geometry, the direction of emission, etc.) and the detector geometry (the components, the sizes, the materials, etc.). In addition, the user code must contain all of the calculations related to the quantities to be obtained.

In this study, we were interested in reproducing real gamma-ray spectra and performing the efficiency calculations. A user code for EGS5 was prepared for this purpose, where the radioactive isotopes comprising the emitting source were modelled through their gamma emission energies and associated probabilities. The source spatial distribution and the emitting directions are set in each simulated history (i.e., in each simulation of the primary source-particles and all of the secondary particles produced by it). Thus, it is possible to define extended sources that emit in the desired directions. Meanwhile, the geometry where the radiation interacts was defined using the combinational geometry package [9], which allows the definition of multiple geometries by combining 14 elemental bodies.

Fig. 1 shows the geometry of the NaI/$LaBr_3$ detectors. The dimensions were adapted to the manufacturer technical specifications. Basically, the geometry was modelled with the corresponding scintillation crystal with a case of 0.5 mm of aluminium. The space between the case and the crystal was filled with air. A glass light guide after the crystal was also considered, and the photomultiplier tube was modelled as a filled-of-air cylinder of aluminium. The material information (density and composition) were taken from [10], and the cut-off energy for the photons and the electrons was set at 10 keV.

2.2.1. Simulation of gamma-ray spectra

When some energy E' is deposited into the detector, a count in the corresponding channel of the spectrum is recorded. However, the gamma-ray spectra obtained in the simulations are very

Fig. 1. Cross-section of the detector geometry used in the simulations. The modelled parts are: scintillation crystal (green), aluminium (grey), glass light guide (red) and air (yellow). (For interpretation of the references to color in this figure legend, the reader is referred to the web version of this article.)

different from the spectra obtained with the detectors due to their finite resolution. Thus, the resolution calibration in the user code must be accounted for obtaining the realistic spectra.

The relationship between the calculated energy deposition spectrum S_0 and the real spectrum S, which would be observed in a real detector, can be represented through the following convolution [11]:

$$S(E) = \int S_0(E') \cdot G(E-E')\mathrm{d}E' \tag{4}$$

where $S_0(E')$ is the probability that a photon deposits the energy E' in the detector crystal per unit energy E' and per incident fluence, and $G(E-E')$ is the probability per unit pulse height that a deposited energy E' will give counts on the energy channel E.

The resolution function $G(E-E')$ is generally approximated by a Gaussian distribution [11]:

$$G(E-E') = \frac{1}{\sqrt{2\pi\sigma^2}} e^{-((E-E')^2/2\sigma^2)} \tag{5}$$

It is important to remark that in Eq. (5), the standard deviation σ is not constant because it is a function of the photon energy, i.e., $\sigma = \sigma(E')$.

The convolution described by Eq. (4) was implemented in the user code using the Box–Muller algorithm [12] to sample the Gaussian functions. Thus, the gamma-particle-deposited energy E' was readjusted using the following equation:

$$E = E' + \sigma(E') \cdot \sin(2\pi\xi_1) \cdot \sqrt{-2\ln\xi_2} \tag{6}$$

where ξ_1 and ξ_2 are independent random variables uniformly distributed in the interval [0,1]. In practice, Eq. (6) is rewritten in terms of the FWHM using the following relationship:

$$\sigma = \frac{\mathrm{FWHM}}{2\sqrt{2\ln 2}} \tag{7}$$

2.2.2. Statistical uncertainty calculations

The results are obtained after the simulation of N_{hist} histories. To estimate the statistical uncertainties, we split these N_{hist} histories into m statistical batches of $N_{hpb} = N_{\mathrm{hist}}/m$ histories. Then, the expected value $\langle x \rangle$ of a certain quantity of interest x is estimated by its average:

$$\bar{x} = \frac{1}{m}\sum_{i=1}^{m} \bar{x}_i \tag{8}$$

where $\bar{x}_i$ is the average of the quantity x_i over the N_{hpb} histories in the i-th batch.

According to the central limit theorem, when $N_{\mathrm{hist}} \to \infty$, the distribution of $\bar{x}$ is Gaussian. Thus, an unbiased estimator of the variance of $\bar{x}$ is

$$s_{\bar{x}}^2 = \frac{s_x^2}{m} \tag{9}$$

with

$$s_x^2 = \frac{1}{m-1}\sum_{i=1}^{m} (\bar{x}_i - \bar{x})^2. \tag{10}$$

For our purposes, the use of the method of statistical batches is unaffected by the problems described in [13] and is fully equivalent to the approach described in [14].

2.2.3. Monte Carlo efficiency calculations

The MC efficiency $\varepsilon_{\mathrm{MC}}$ calculations were performed by reproducing the experimental setup for each radioactive source (to account the different source sizes and source-detector distances). For the efficiency calculations, a monoenergetic source was considered to avoid unnecessary interferences in the spectrum. Thus, the MC efficiency was calculated in each statistical batch as

$$\varepsilon_{\mathrm{MC}} = \frac{N_{\mathrm{counts}}}{N_{hpb}} \tag{11}$$

where N_{counts} is the number of counts under the full energy peak, and N_{hpb} is the number of photons emitted by the source per batch. Then, the MC efficiency and its uncertainty were obtained from Eqs. (8) and (9).

2.2.4. Variance reduction

To obtain better statistics with fewer simulations, a variance reduction method, the direction bias method [14], was implemented, which only considers the photons that are emitted against the detector. In this method, the scored quantities must be weighted with the corresponding statistical weight w. The weight is defined in each history as

$$w = \frac{\text{true probability}}{\text{sampled probability}} \tag{12}$$

2.3. Activity calculation

Once the MC efficiencies $\varepsilon_{\mathrm{MC}}$ are calculated, it is possible to estimate the activity of any radioactive isotope. If we use n_p peaks for the calculation, the activity A_{calc} of the given isotope is the weighted mean of all k-peak activities $A_{\mathrm{calc},k}$:

$$A_{\mathrm{calc}} = \frac{\sum_k^{n_p} A_{\mathrm{calc},k} \cdot w_k}{\sum_k^{n_p} w_k} \tag{13}$$

with the weights

$$w_k = \frac{1}{(\delta A_{\mathrm{calc},k})^2} \tag{14}$$

Then, the uncertainty of Eq. (13) is evaluated using the following relationship:

$$\delta A_{\mathrm{calc}} = \frac{1}{\sqrt{\sum_k^{n_p} w_k}} \tag{15}$$

The activity related to the k-peak is calculated by rearranging Eq. (2) as

$$A_{\mathrm{calc},k} = \frac{N_k}{\varepsilon_{\mathrm{MC},k} \cdot t \cdot p_k} \tag{16}$$

where N_k is the number of counts under the k-peak, p_k the probability and $\varepsilon_{\mathrm{MC},k}$ is the corresponding efficiency.

Finally, the uncertainty for the k-peak corresponding activity is given by

$$\delta A_{\mathrm{calc},k} = A_{\mathrm{calc},k}\sqrt{\left(\frac{\delta N_k}{N_k}\right)^2 + \left(\frac{\delta \varepsilon_{\mathrm{MC},k}}{\varepsilon_{\mathrm{MC},k}}\right)^2 + \left(\frac{\delta p_k}{p_k}\right)^2} \tag{17}$$

3. Results and discussion

3.1. Energy calibrations

To set the suitable n for Eq. (1) and to obtain the fitting coefficients, several data points were obtained with the available radioactive sources described in Table 1. Fig. 2 shows the data used for NaI(Tl) and $LaBr_3$(Ce) in the energy calibrations.

Table 2 shows the results of the data fit to Eq. (1) for $n=1$, 2, 3 and 4. The goodness of fit was evaluated with the adjusted coefficient of determination $\overline{R}^2$ instead of the usual coefficient of determination R^2. This coefficient takes into account whether the additional fitting parameters in fact improve the fit.

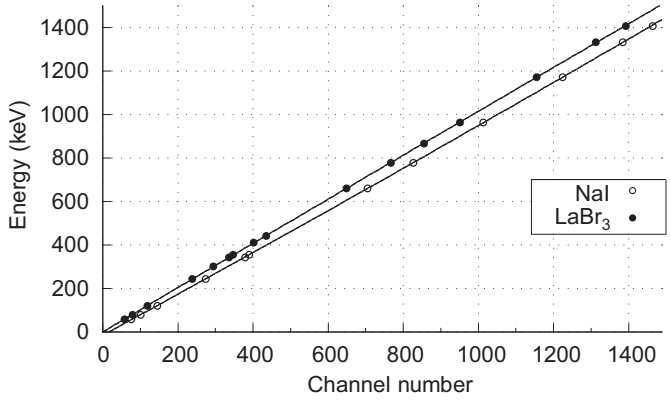

Fig. 2. Data points used for the energy calibration of both the NaI(Tl) and the $LaBr_3$(Ce) detectors. The continuous lines correspond to a 2nd-order polynomial fit.

Table 2
Fitting functions for the energy calibration with their corresponding adjusted coefficient of determination for both detectors.

Fitted $E(C)$ function	$\overline{R}^2$	
	NaI	$LaBr_3$
$E=a_0+a_1C$	0.999968	0.999995
$E=a_0+a_1C+a_2C^2$	0.999994	0.999996
$E=a_0+a_1C+a_2C^2+a_3C^3$	0.999994	0.999996
$E=a_0+a_1C+a_2C^2+a_3C^3+a_4C^4$	0.999993	0.999997

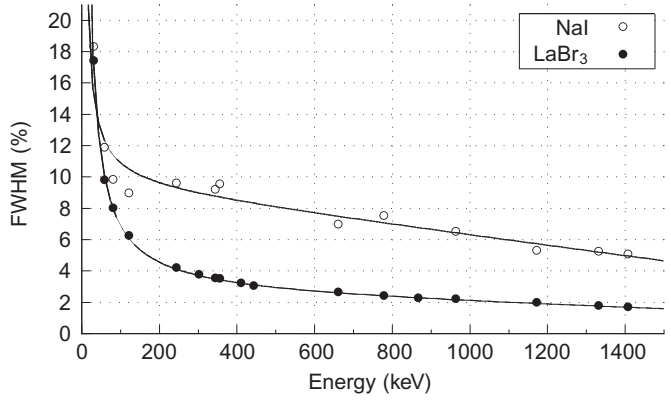

Fig. 3. Data points used in the resolution calibration of both the NaI(Tl) and the $LaBr_3$(Ce) detectors. The continuous lines correspond to a 2nd-order polynomial fit.

The results in Table 2 show that a 2nd-order polynomial ($n=2$) is the best option for the energy calibration. However, for $n=1$, the detectors showed a good linearity in all ranges. The highest deviation from linearity was produced at the lowest energy (59.5 keV), but it was less than 12% and 4% for NaI and $LaBr_3$, respectively. Finally, for $n>2$, the fit did not improve significantly, but deviations lower than 2% for the lowest energy point could be achieved.

3.2. Resolution calibrations

To identify the best FWHM(E) function, different functions were tested to fit the data in Fig. 3. Again, the accuracy of the fit was evaluated with the adjusted coefficient of determination $\overline{R}^2$. The results of different fits are shown in Table 3.

Table 3
Fitted functions with their corresponding adjusted coefficient of determination for both detectors. The references of the functions found in the literature for different types of gamma-spectrometers are also provided.

Fitted FWHM function	Literature		$\overline{R}^2$	
	Detector	References	NaI	$LaBr_3$
$FWHM(E)=a+bE$	Ge	[3,21]	0.98011	0.99301
$FWHM(E)=a+b\sqrt{E}$	Ge	[3]	0.99534	0.99904
$FWHM(E)=a\cdot E^b$	NaI	[15]	0.99310	0.99884
$FWHM(E)=a+b\sqrt{E+cE^2}$	NaI, $LaCl_3$	[16-18]	0.99581	0.99900
$FWHM(E)=a\sqrt{E}+bE$	NaI, $LaBr_3$	[3,19]	0.99138	0.99873
$FWHM(E)=a\sqrt{E}$	NaI	[20]	0.98729	0.99850
$FWHM(E)=\sqrt{a+bE}$	NaI, Ge	[3,21]	0.97922	0.99923
$FWHM(E)=\sqrt{a+bE+cE^2}$	Ge	[3,21]	0.91769	0.99917
$FWHM(E)=a+bE+cE^2$	NaI, $LaBr_3$	[22]	0.99713	0.99979
$FWHM(E)=a+b\sqrt{E+c}$	NaI, $LaBr_3$	This study	0.99492	0.99922
$FWHM(E)=a+bE+cE^2+d\sqrt{E}$	NaI, $LaBr_3$	This study	0.99699	0.99980
$FWHM(E)=a+bE+c\sqrt{E}$	NaI, $LaBr_3$	This study	0.99550	0.99904
$FWHM(E)=aE+bE^2$	NaI, $LaBr_3$	This study	0.99695	0.98146

From the results of Table 3, the relationship that best fits the experimental data for both detectors is

$$FWHM(E)=a+bE+cE^2 \quad (18)$$

Eq. (18) also has a more user-friendly mathematical form than other equations, which makes it more usable. The results in Table 3 show that the data points from the $LaBr_3$ detector provide better fits in comparison with the NaI detector. This result is obvious from the distribution of the data points observed in Fig. 3, which is more irregular for NaI. Similar results were obtained by other authors [8].

From Fig. 3, the energy resolution is clearly better for the $LaBr_3$ detector than for the NaI detector all over the energy range. In particular, the obtained resolutions for the 661.7 keV γ-rays of the ^{137}Cs source were 7.0% for the NaI detector and 2.6% for the $LaBr_3$ detector. However, at low energies the differences become smaller. This can be explained by considering that the energy resolution improves when the light yield increases. Thus, at low energies NaI crystals show an excess of light [1,8], while the $LaBr_3$ ones show a reduced light yield in this region [6]. And so, this non-proportionality of the light yield explains the observed behaviour.

3.3. Spectra simulations

The resolution function obtained from the fit of Eq. (18) for each detector was incorporated into the MC code. As the fit can only be trusted in the energy region $[E_{min},E_{max}]$ defined by the calibration sources, we impose a linear interpolation from FWHM(0)=0 to FWHM(E_{min}). The correct performance of the implemented algorithm can be observed in Fig. 4 for an ^{152}Eu source.

3.4. Efficiency calculations

The efficiency calculations of the MC code were tested with the certified sources described in Table 1. Table 4 shows the source-detector distance considered, the experimental and the calculated efficiencies, ε_{exp} and ε_{MC}, and the relative differences RD (%) for both detectors.

From Table 4, we observe that the simulations are in good agreement with the experimental measurements. The discrepancies between the experimental and the calculated efficiencies can

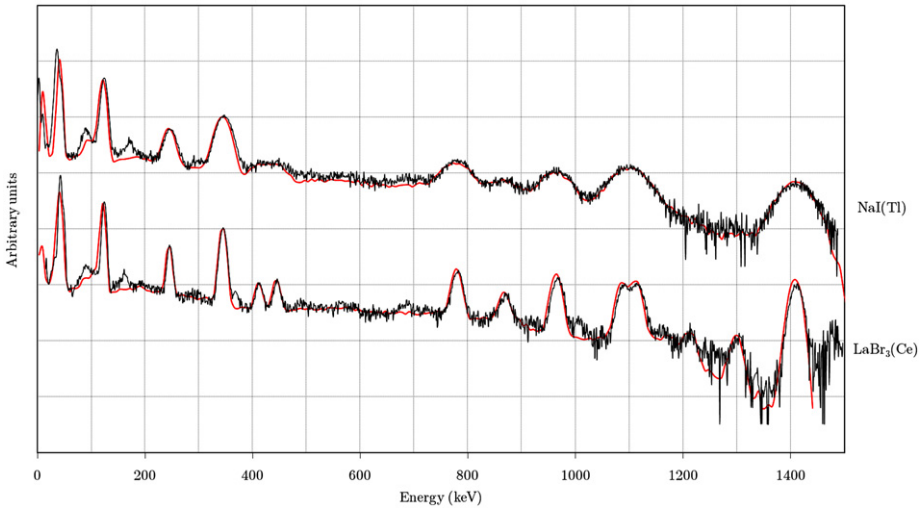

Fig. 4. Experimental (black) and simulated (red) spectra for both detectors, NaI(Tl) and $LaBr_3$(Ce). For purposes of comparison, the spectra are displayed in arbitrary units. (For interpretation of the references to color in this figure legend, the reader is referred to the web version of this article.)

Table 4
Comparison of the experimental and the MC-simulated efficiencies of both detectors.

Radionuclide	Source-detector distance (cm)	Energy (keV)	NaI			$LaBr_3$		
			ε_{exp} (%)	ε_{MC} (%)	RD (%)[b]	ε_{exp} (%)	ε_{MC} (%)	RD (%)[b]
^{241}Am	5	59.541	2.5(3)	2.570(4)	−2.9	3.0(3)	3.090(7)	−2.8
^{133}Ba	5	80.998[a]	3.2(3)	3.141(6)	1.5	3.8(4)	3.576(6)	7.0
		302.851	n.a.	n.a.	n.a.	2.0(2)	2.013(6)	−1.6
		356.013	1.5(2)	1.506(5)	−0.5	1.8(2)	2.013(6)	−14.2
^{137}Cs	5	661.657	1.0(1)	1.045(3)	−2.4	1.3(1)	1.308(4)	−0.9
^{60}Co	2	1173.228	1.3(1)	1.302(6)	−3.0	2.1(2)	2.149(8)	−3.2
		1332.492	1.2(1)	1.141(5)	1.7	2.0(2)	1.897(9)	3.4

[a] For the 80.998 keV energy of ^{133}Ba, we also took into account the contribution of the 79.61 keV line.
[b] $RD(\%) = \frac{\varepsilon_{exp}-\varepsilon_{MC}}{\varepsilon_{exp}} \times 100$.

be associated with many factors such as source positioning, detector modelling, the inaccuracy of the manufacturer parameters, the activities of the reference sources and true coincidence summing. Consequently, these factors may make our simulation results for the $LaBr_3$(Ce) not as accurate as the NaI(Tl) results.

Most of these discrepancies could be reduced by positioning the radioactive reference sources farther away from the detector; thus, it would be desirable to have reference sources of higher activity.

Finally, it is important to remark that the MC uncertainties are small because they are only statistical. In fact, they can be reduced even by increasing the number of simulated histories. Thus, MC uncertainties must be only taken as indicators of good statistics in the simulations.

3.5. Activity calculations

From the MC efficiencies given in Table 4, we used Eq. (13) to estimate the activities of the radioactive sources. Table 5 shows the calculated activities and the relative differences RD (%) for both detectors.

The results included in Table 5 show good agreement between the certified activity of the radiation sources and the calculated activities obtained from the MC efficiencies. Thus, the maximum relative differences between the current and the calculate activity were less than 3.4% in absolute value. The observed discrepancies can be attributed to the same factors discussed in Section 3.4.

The uncertainties provided with the calculated activities are low due to the small uncertainties associated with MC efficiencies. Thus, if the method was used to estimate unknown activities, it would be necessary to assume a higher uncertainty to take into account the other possible sources of uncertainty.

Table 5
Comparison of the certified activities with the activity calculations for both detectors.

Radionuclide	Current activity[a] (kBq)	NaI		$LaBr_3$	
		Calculated activity (kBq)	RD(%)[b]	Calculated activity (kBq)	RD(%)[b]
^{241}Am	3.2 ± 0.3	3.12 ± 0.03	2.8	3.12 ± 0.03	2.7
^{133}Ba	1.0 ± 0.1	1.02 ± 0.02	−1.1	0.97 ± 0.01	3.4
^{137}Cs	4.0 ± 0.4	3.93 ± 0.05	2.3	3.98 ± 0.04	0.9
^{60}Co	1.40 ± 0.14	1.40 ± 0.02	0.2	1.41 ± 0.01	−0.5

[a] At the time of measurement.
[b] $RD(\%) = \frac{A-A_{calc}}{A} \times 100$.

4. Conclusions

In this study, we presented a complete calibration (energy, resolution and efficiency calibrations) of two scintillation detectors, NaI(Tl) and $LaBr_3$(Ce), to be used in gamma-spectrometry.

For the energy calibration, we found that the best function to establish the energy-channel relation is a 2nd-degree polynomial. After testing several fitting functions for the resolution calibration, we found that the best fitting function for the FWHM(E) relation was also a 2nd-degree polynomial.

Additionally, an MC user code for the EGS5 code system was developed and validated to reproduce a realistic gamma-ray spectra and efficiency calculations for both the NaI(Tl) and $LaBr_3$(Ce) detectors. The correct implementation of the FWHM function in the MC code was tested across all the energy ranges by comparing the simulated spectra with the experimental spectra. We also validated the code by calculating the efficiency of simple source geometries, and the calculated efficiencies were in good agreement with the experimental values obtained from certified radioactive sources. Finally, using the calculated efficiencies in the activity calculations also provided good results.

The validation of this MC user code for simple source geometries will permit one to extrapolate the calculations to other distributions of radioactive sources. Thus, the code can be used to calculate the efficiencies for different kinds of extended sources and to estimate their activities.

Acknowledgements

Part of this research has been performed using the resources of CESCA (Centre de Supercomputació de Catalunya).

References

[1] M. Moszyński, Nuclear Instruments and Methods A 505 (2003) 101–110.
[2] BrilLanCe^{TM} Scintillators Performance Summary (Revision: January, 2009). Saint-Gobain Crystals, Scintillation Products. Available: 〈http://www.detectors.saint-gobain.com/uploadedFiles/SGdetectors/Documents/Technical_Information_Notes/BrilLanCe-Scintillators-Performance-Summary.pdf〉.
[3] G. Gilmore, Practical Gamma-Ray Spectrometry, 2nd edn., John Wiley & Sons Ltd, England, 2008.
[4] Update of X Ray and Gamma Ray Decay Data Standards for Detector Calibration and Other Applications. Volume 1: Recommended Decay Data, High Energy Gamma Ray Standards and Angular Correlation Coefficients. International Atomic Energy Agency. Vienna, 2007. Available: 〈http://www-pub.iaea.org/MTCD/publications/PDF/Pub1287_Vol1_web.pdf〉.
[5] F. Quarati, A.J.J. Bos, S. Brandenburg, C. Dathy, P. Dorenbos, S. Kraft, R.W. Ostendorf, V. Ouspenski, A. Owens, Nuclear Instruments and Methods A 574 (2007) 115–120.
[6] M. Moszyński, Ł. Świderski, T. Szczęśniak, A. Nassalski, A. Syntfeld-Każuch, W. Czarnacki, G. Pausch, J. Stein, P. Lavoute, F. Lherbert, F. Kniest, IEEE Transactions on Nuclear Science 55 (2008) 1774–1780.
[7] M. Moszyński, A. Nassalski, A. Syntfeld-Każuch, Ł. Świderski, T. Szczęśniak, IEEE Transactions on Nuclear Science 55 (2008) 1062–1068.
[8] M. Balcerzyk, M. Moszyński, M. Kapusta, Nuclear Instruments and Methods A 537 (2005) 50–56.
[9] H. Hirayama, Y. Namito, A.F. Bielajew, S.J. Wilderman, W.R. Nelson, The EGS5 Code System, SLAC-R-730 and KEK Report 2005-8, 2005.
[10] M.J. Berger, J.S. Coursey, M.A. Zucker, J. Chang, ESTAR, PSTAR, and ASTAR: Computer Programs for Calculating Stopping-Power and Range Tables for Electrons, Protons, and Helium Ions (version 1.2.3), National Institute of Standards and Technology, Gaithersburg, 2005. Available: 〈http://physics.nist.gov/Star〉.
[11] ICRU Report 53, International Commission on Radiation Units and Measurements, Bethesda, Maryland, 1994.
[12] G.E.P. Box, M.E. Muller, Annals of Mathematical Statistics 29 (1958) 610–611.
[13] B.R.B. Walters, I. Kawrakow, D.W.O. Rogers, Medical Physics 29 (2002) 2745–2752.
[14] S. Hurtado, M. García-León, R. García-Tenorio, Nuclear Instruments and Methods A 518 (2004) 764–774.
[15] H.X. Shi, B.X. Chen, T.Z. Li, D. Yun, Applied Radiation and Isotopes 57 (2002) 517–524.
[16] K. Amgarou, C. Domingo, T. Bouassoule, F. Fernandez, Nuclear Instruments and Methods B 267 (2009) 2944–2951.
[17] V. Kovaltchouk, R. Machrafi, Annals of Nuclear Energy 38 (2011) 788–793.
[18] S. Baccouche, D. Al-Azmi, N. Karunakara, A. Trabelsi, Applied Radiation and Isotopes 70 (2012) 227–232.
[19] G. Anil-Kumar, I. Mazumdar, D.A. Gothe, Nuclear Instruments and Methods A 609 (2009) 183–186.
[20] S. Ashrafi, S. Anvarian, S. Sobhanian, Journal of Radioanalytical and Nuclear Chemistry 269 (2006) 95–98.
[21] S. Hurtado, M. Garcia-Leon, R. Garcia-Tenorio, Nuclear Instruments and Methods A 564 (2006) 295–299.
[22] G. Su, Z. Zeng, J. Cheng, Radiation Protection Dosimetry 146 (2011) 103–106.